CEAS Space Journal
https://doi.org/10.1007/s12567-024-00574-8

ORIGINAL PAPER

Design, manufacturing, and assembly of the GRASS small body gravimeter spring

Matthias Noeker[1,2] · **Birgit Ritter**[1] · **Emiel Van Ransbeeck**[3,4] · **Özgür Karatekin**[1]

Received: 21 December 2023 / Revised: 18 October 2024 / Accepted: 29 October 2024

Abstract

The GRAvimeter for small Solar System bodies (GRASS) is a novel spring-based gravimeter for the application in extremely low-gravity environments on small bodies in our Solar System. It is one of the Juventas CubeSat payloads as part of the ESA Hera mission to measure the surface gravity on the asteroid moon Dimorphos. The GRASS gravimeter was successfully launched on-board Hera on 7 October 2024. Key element of this instrument is the gravimeter spring, a cantilever-type bending spring, allowing for measurements at arbitrary instrument orientation. This paper presents the design, manufacturing, and integration of the developed sensing element assembly. The spring design can serve as a future reference for data analysis of the gravimeter data obtained in-situ on extraterrestrial surfaces. The manufacturing process is detailed, including the raw material, laser cutting, heat treatment, and gold sputtering. The step-by-step assembly describes the integration of the spring assembly which includes the clamping of the spring and the tip mass, added to the spring to realise larger deflections and henceforth increase the sensitivity of the instrument for the small body gravity environment.

Keywords Gravimeter · Spring · Bending spring · Space gravimeter · Small bodies · Hera mission · GRASS · Didymos · Dimorphos · Instrumentation · Sensor

1 Introduction

Surface gravimetry is a well-known geophysical exploration technique on Earth, yet the application on extraterrestrial surfaces throughout the Solar System remained a rarity. So far, only two dedicated gravimeter experiments have been sent to outer space: The Lunar Surface Gravimeter (LSG) [1] and the Traverse Gravimeter Experiment (TGE) [2] were part of the Apollo 17 mission, of which only the latter succeeded to return surface gravity measurements. The TGE was a vibrating string accelerometer (VSA) and the LSG was a spring-based gravimeter. Additionally, using on-board accelerometers, [3] inferred gravimetric data from the Curiosity rover acceleration data along the vehicles traverse on the Red Planet. While not equipped with a dedicated gravimeter, the rover carried (primary and backup) see LN-200S and LN-200S HP Inertial Measurement Units | Northrop Grumman Rover Inertial Measurement Units (RIMUs), each equipped with three-axis solid-state silicon MEMS accelerometers.

The GRAvimeter for small Solar System bodies (GRASS) is a newly developed spring-based gravimeter for asteroid surface gravimetry. Integrated into the Juventas CubeSat [4]

Matthias Noeker is now at the German Space Agency at DLR in Bonn, Germany

✉ Matthias Noeker
matthias.noeker@observatory.be

Birgit Ritter
birgit.ritter@observatory.be

Emiel Van Ransbeeck
emiel.vanransbeeck@skynet.be

Özgür Karatekin
ozgur.karatekin@observatory.be

[1] Royal Observatory of Belgium, Ringlaan-3-Avenue Circulaire, Ukkle, Brussels 1180, Belgium

[2] Université catholique de Louvain, 1-Place de l'Université, Ottignies-Louvain-la-Neuve 1348, Belgium

[3] VRE Consultancy, Dries 15, Mazenzele 1745, Belgium

[4] Royal Belgian Institute for Space Aeronomy, Ringlaan-3-Avenue Circulaire, Uccle, Brussels 1180, Belgium

Published online: 30 November 2024

as part of the ESA Hera mission [5], GRASS will measure the surface gravity of Dimorphos, the asteroid moon of Didymos. Together with Hera, GRASS was successfully launched on 7 October 2024. With this, it will contribute to the science requirements (a) to determine the mass of Dimorphos and the dynamical properties of the Didymos system, and (b) to constrain the interior structure of Dimorphos. For the instrument development, the challenging reference gravity of $4.5 \cdot 10^{-5} m/s^2$ has been considered, being 5 orders of magnitude smaller than the terrestrial gravity. The final mission phase inside the binary asteroid system will consist of a ballistic landing on the asteroid moon Dimorphos. Here, the landing attitude will not be controlled actively and several bounces are expected before settling of the spacecraft [6], similarly to the Philae landing(s) on comet 67P/Churyumov-Gerasimenko [7].

Here, we concentrate on the design constraints, spring manufacturing, and assembly of those blades. This paper first describes and explains the gravimeter spring design and design constraints (Sect. 2). Further, the technical details on the manufacturing steps (Sect. 3) and the integration of the spring assembly (Sect. 4) of this novel gravimeter spring type are presented. Finally, possible future adaptations of the spring are discussed in Sect. 5 before this work is concluded in Sect. 6.

The presented GRASS gravimeter spring description forms the second part in a mini-series of the mechanical gravimeter design description. Following the presentation of the gravimeter rotation mechanism [8], it is envisioned to describe likewise the electro-mechanical displacement transducer design. The sensor head with the structural cradle part, hosting the here-described spring assembly, will be mentioned briefly in this work. It ensures the full functionality of the gravimeter, allowing to measure the spring deflection under gravity, and complements the triad together with the spring assembly and rotation mechanism.

2 Spring design and design constraints

2.1 Spring design constraints

The spring design constraints were driven by the overall GRASS instrument design, which in turn was constrained by the overall accommodation budgets available inside the 6U-XL-CubeSat. For reference, the available volume budget was to fit inside 1 CubeSat unit ($1\,\mathrm{U} = (100\,\mathrm{mm})^3$) and the spring-bearing sensor head diameter (so-called: cradle) was limited to a diameter of 15 mm [8]. The maximum permissible instrument length was set to 99 mm, to provide 0.5 mm clearance on both instrument ends. Inside the cradle, the overall spring assembly (Sect. 4) had a strict length limitation of 58 mm.

The acting gravity will be inferred from measuring the spring deflection. This will be realised by means of differential capacitance. Placing the (flat) spring in-between two electrodes, two parallel plate capacitors are formed, consisting of the two pairs Electrode-1/Spring and Spring/Electrode-2. To optimise the sensitivity, this measurement will take place at the part of the spring farthest away from the rigid clamp. As will be further discussed in Sect. 3, this setup requires excellent parallel alignment of the spring and the electrodes (sensor head) while minimising the separation of electrodes to maximise the capacitive sensitivity.

Considering the above-mentioned design constraints, paired with the overall capability of being integrated into the GRASS gravimeter, as further described in [9], the GRASS gravimeter spring design has been developed. The choice of the flat spring will be justified in the next Subsection, together with the presentation of the precise dimensions of the overall spring assembly. Following this, the influence of key design variables on the spring deflection will be presented in Sect. 2.3, before the eigenfrequency of the spring is computed (Sect. 2.4).

2.2 Spring rationale

Due to both the unknown landing attitude and the unknown gravity vector orientation, a specific solution to obtain the surface gravity vector in 3D space has been developed. With the aid of a payload rotation mechanism [8, 10], two orthogonally aligned springs are rotated, such that their deformation can be each described by a sinusoidal wave. This does not only allow the 3D gravity vector reconstruction, but likewise allows measurement bias rejection due to the periodical inversion of the measurement direction.

Generally, in absence of a levelling mechanism and for bias rejection, the design needs to allow the rotation of the spring, such that the (sensitive) measurement direction is periodically inverted. Obviously, a classical helical spring with a test mass cannot be simply flipped upside down. Placing a mass in between one (or more) pairs of springs would work, but drastically increases the required volume if such setup needs to be rotated. Alternatively, a bending spring in the form of a cantilever beam (Fig. 1) is better suited, as placing the spring in an upside-down position will result in the same deformation but towards the other side of the spring. Here, the required volume of revolution will be significantly smaller.

The accelerometer system quasi-steady acceleration measurement (QSAM) [11] onboard the Spacelab inverted the measurement direction periodically, i.e., rotated the measurement device by 180 degrees, for bias rejection. As stated above, the bias rejection alone, however, is not sufficient for the GRASS application. With both the landing attitude and the gravity vector orientation on the surface of

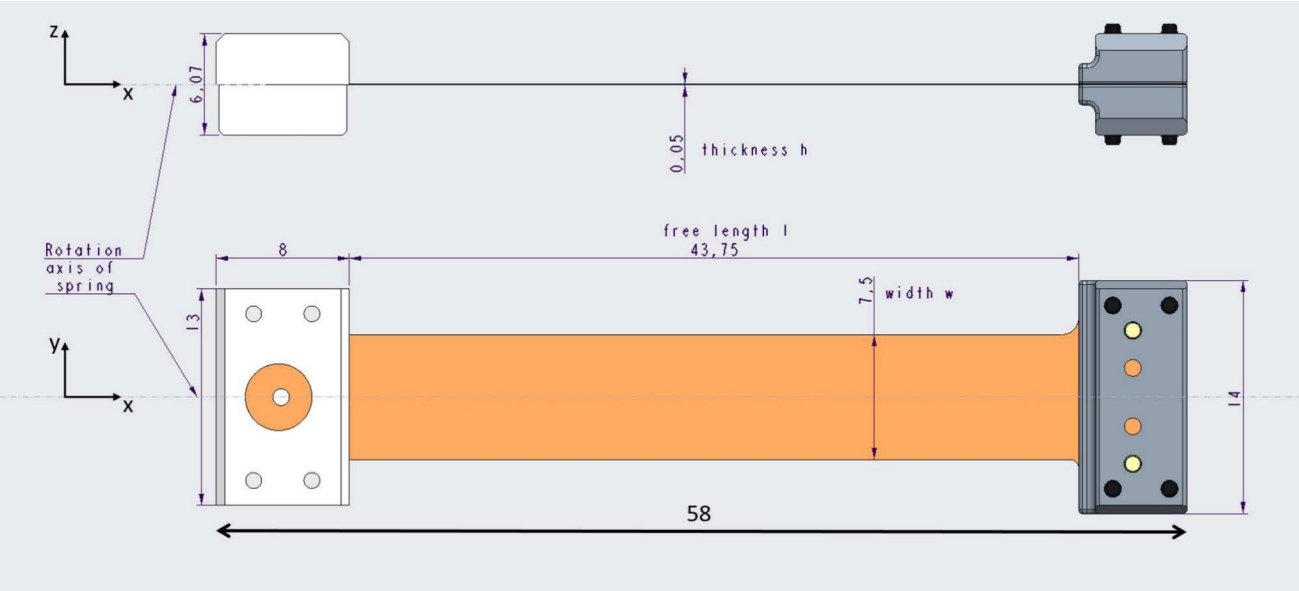

Fig. 1 Gravimeter spring design with indicated rotation axis (i.e., the long axis of the spring), and width w, free length l, and thickness h indicated. The coordinate systems indicates the sensitive ($\pm z$), and the two insensitive ($\pm x$ and $\pm y$) directions. The left end of the spring is clamped in Macor®, a ceramic material, for electrical insulation and the right end with increased width is the so-called *tip mass* to increase the spring deflection and thus sensitivity. All dimensions are given in mm

Dimorphos unknown, the angular separation between the measurements should be (much) smaller than 180 degrees. For such measurements at incremental rotation, however, the spring should be sensitive in one measurement dimension and insensitive in the other two dimensions. Here, the third dimension ($\pm x$, Fig. 1) is the elongation of the spring along its long axis, which can be excluded from the further discussion, as it can be easily shown that this is much smaller than the bending. The spring deflection with the aim to maximise the sensitivity in one dimension while minimising it in the other of the two remaining dimensions will be discussed in the next subsection.

2.3 Spring deflection

Regarding the two orthogonal bending directions, the combination of a sensitive ($\pm z$, Fig. 1) with an insensitive dimensions ($\pm y$, Fig. 1) is best achieved with a flat-bending spring, i.e., with a bending spring of rectangular cross-section. Here, one dimension of the rectangle should be much larger than the other dimension. Other cross-sections, such as hollow-rectangular profiles, would also comply with this requirement, but with more material further away from the neutral axis, the sensitivity of the spring would be reduced, while being more complex to manufacture and larger in volume. On the contrary, a round bending spring (rod) would be equally sensitive in both dimensions, or, generally speaking, all possible bending directions.

It is recalled that the deformation of a spring is directly proportional to the (weight) force $F = m \cdot a$ acting on it, where m is the mass acting on the spring and the acceleration a is, in this application, the gravity g_0. Note that the spring will also deform under its own weight. Clearly, the maximum deflection of a bending spring increases with the overall length of the spring. Moreover, the deformation of a cantilever beam (spring) is inversely proportional to its second moment of area I, and therefore, it is required to minimise this quantity [Eq. (1)] to obtain a maximum deflection, and therefore sensitivity in the gravimeter spring

$$I = \frac{wh^3}{12}, \tag{1}$$

where h is the thickness of the spring, and w is the free width of the spring. Free width like free length refers to the part of the spring that is neither clamped nor equipped with a tip mass, i.e., *free to deform*.

Using a rectangular cross-section, the second moment of area I can be minimised by minimising the spring thickness h (cubic influence). The width w should also be as small as possible, but can be larger to provide the structural stability, as it only provides a directly proportional influence. With the dimensions given in Fig. 1, the ratio of width w to thickness h is $7.5\,\text{mm}/0.05\,\text{mm} = 150$. The large ratio of width to thickness becomes likewise visible in Fig. 1, with the spring being barely visible in the side view. The second moment of area of the spring is calculated in Eq. (2)

$$I = \frac{0.0075\,\mathrm{m} \cdot (5 \cdot 10^{-5}\,\mathrm{m})^3}{12} = 7.8125 \cdot 10^{-17}\,\mathrm{m}^4. \quad (2)$$

If the spring is now rotated by 90 degrees from its most sensitive setting (gravity aligns with the thickness dimension), the second moment of area changes, such that the width and thickness are exchanged with regard to the bending direction. The much larger width now has a cubic influence and minimises the sensitivity in the second direction. This is sketched in Fig. 2. The increased second moment of area is calculated in Eq. (3), showing that the deflection in the insensitive direction will be 5 orders of magnitude smaller than the deformation in the sensitive direction of the spring

$$I = \frac{5 \cdot 10^{-5}\,\mathrm{m} \cdot (0.0075\,\mathrm{m})^3}{12} = 1.7578 \cdot 10^{-12}\,\mathrm{m}^4. \quad (3)$$

Generally, if the bending spring is clamped on one side, forming a cantilever, it already forms a gravimeter spring due to its own weight. For very small gravity environments such as on small bodies, however, it is required to increase the deflection by addition of a high-density test mass (hereafter: *tip mass*) at the free hanging end of the spring (also called *blade*). Neglecting the own mass of the free spring of about 0.135 g compared to more than 8 g of the tip mass (see below), the deflection can be considered directly proportional to the mass of the tip mass.

This is achieved by the addition of two test masses in tungsten on the spring clamp-far end. To protect the spring during launch vibration and (separation/landing) shock, the tip mass is equipped with Vespel®-made dampers. Vespel® is a high-performance durable polymide commonly used in space applications. The Vespel® parts protect the tip mass (and thus the spring) from contact with the surrounding gravimeter sensor head structure. This avoids metal–metal contact, hindering cold welding which would end the movement of the spring and bypass the electrical insulation of the spring from the cradle. The manufacturing of the spring as core element of the spring assembly is introduced in the next section and the assembly integration, with a more detailed description of the further assembly elements, will be presented in Sect. 4. These considerations lead to the presented design of the GRASS gravimeter spring. The general gravimeter spring concept is herewith introduced, with the dimensions as actually used for the ESA Hera mission. These numbers can therefore serve as a reference for future data analysis of the data to be returned by the GRASS gravimeter.

2.4 Eigenfrequency

Using the measured mass of the two tip mass halves being $2 \times 4.178\,\mathrm{gram} = 8.356\,\mathrm{gram}$, it is possible to calculate the eigenfrequency of the gravimeter spring. Since the mass of the deforming spring is less than 0.135 g, more than 60 times less than the tip mass, the eigenfrequency f_1 of the spring can be computed according to [12], under negligence of the own weight of the spring [Eq. (4)]

$$f_1 = \frac{\sqrt{3}}{2\pi}\sqrt{\frac{EI}{l^3 M}}, \quad (4)$$

where E is the Young's modulus of the spring (131 GPa for CuBe), I has been introduced in Eq. (1), l is the free length of the spring (Fig. 1), and M is the above-mentioned mass of the tip mass. The masses of the dampers, spring pins, and glue can be neglected here. With this, the eigenfrequency is as follows:

$$f_1 = 1.054\,\mathrm{Hz}. \quad (5)$$

This value is important, as the linear response to non-static accelerations is only given below the first eigenfrequency of the sensing device. The low eigenfrequency of the spring, however, is not problematic regarding the vibration

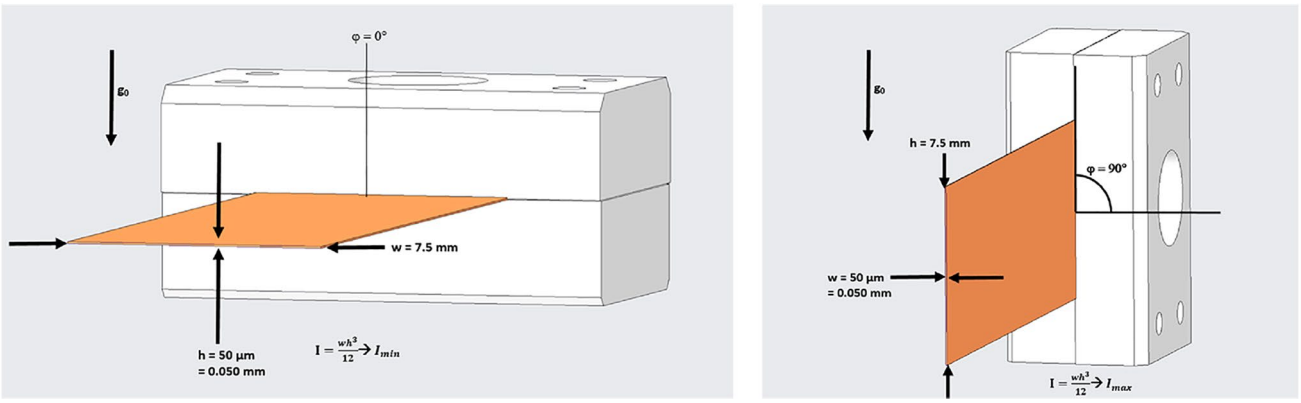

Fig. 2 Second moment of area for the sensitive (left) and insensitive (right) directions, rotated by 90 degrees

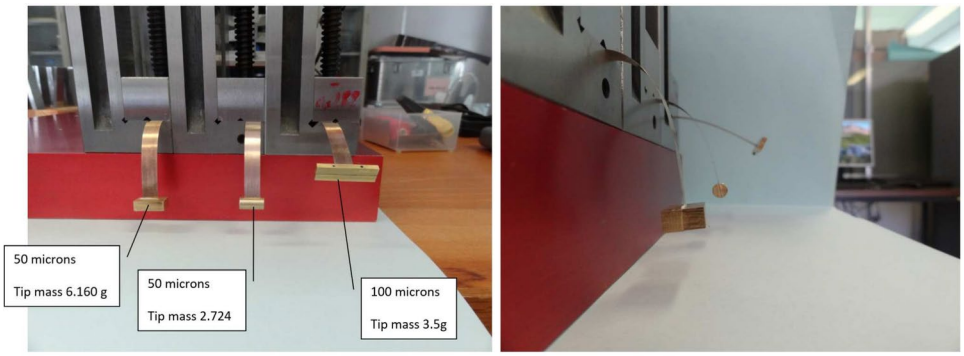

Fig. 3 (Left) Front-top and (right) side view of a spring deflection experiment under (Earth) gravity. Between the two springs with 50 micron thickness, a difference in deflection is visible. A significant reduction in this level of deflection is achieved by the third spring which has a thickness of 100 micron, twice the thickness of the other two springs

environment, as the actual spring setup in the vibration environment is damped. This value thus has only relevance with regards to measuring (variable) surface gravity.

A good illustration of the two main spring design drivers, the mass of the tip mass and this spring thickness, influencing the sensitivity of the instrument, and thus the overall science performance is given in Fig. 3. A qualitative deflection test of two identical springs with different tip mass, and a third spring with twice the thickness with a tip mass between the two other masses is shown. Clearly, the deflection under Earth gravity cannot be scaled to the micro-gravity environment, as such large deflection will always exhibit non-linearities. From a qualitative point of view, however, the (small but visible difference) due to the tip mass is clearly much less significant than the difference due to the thickness of the spring.

3 Spring manufacturing

The production of the (flat) bending spring was the prime challenge. As introduced in Sect. 2.1, the spring deflection is measured by means of a capacitive transducer. For this, the spring will be placed centred and parallel between two parallel electrodes. From a parallel plate capacitor, we know that the capacitance will be maximised by minimising the plate (here: *electrode*) separation. At the same time, a cantilever spring is most sensitive at its tip, i.e., at the largest distance from the (rigid) clamp. Therefore, the spring had to be machined with a flatness in the micrometre range to ensure a parallel alignment of the spring with the electrodes at the distance farthest away from the clamp. The maximum permissible non-straightness tolerance of the spring was set to $\pm 5 \mu m$. Since this also includes the geometric tolerances on the clamp (Sect. 4.2), the demand to the machined spring is even tighter. This straightness in the order of microns had to be realised over the free length of 43.75 mm.

In this section, all steps of the GRASS gravimeter spring manufacturing will be presented in chronological order. Starting from the raw material (Sect. 3.1), the laser cutting is subsequently discussed in Sect. 3.2. After this, the heat treatment of the sensing element is discussed (Sect. 3.3), and finally, the gold sputtering is described in Sect. 3.4. The manufacturing of the tip mass and clamp is, albeit the high demands on tolerances and machining quality, a standard manufacturing procedure and not explained in this section. Relevant steps regarding the integration and the herewith related high demands on (geometric) machining tolerances are reported in the next section.

The dimensions of all used parts were always verified upon delivery. Here, we note the error limit (DIN 863-1) of the digital micrometre *Micromar 40 EWR* (used to measure critical dimensions) to be 2 microns for the measuring range from 0 to 25 mm with a resolution of 1 micron.

3.1 Raw material

For the flat-bending spring design, the Copper Beryllium (CuBe) alloy has been selected for very good spring properties. Elasticity is here combined with high strength and a high resistance against stress relaxation.[1]

We obtained the foil raw material Cu98/Be 2 with temper half hard and with a nominal thickness of 0.050 mm = 50 micron. The key material properties are listed in Table 1 as provided by the supplier. Clearly, some properties are provided with rather large ranges, demanding additional calibration steps for the (gravimeter) spring application. This is not done on spring level, but rather on the gravimeter instrument level, as part of the overall payload characterisation. As the material was rolled, the supplier was asked to clearly mark the direction of rolling on the sheet material. The appearance of the raw material and (part of) the indication arrow (marker) of the rolling direction are visible in Fig. 4.

[1] https://www.matthey.ch/fileadmin/user_upload/downloads/Fichiers_PDF/GuideToCopperBeryllium_EN.pdf, accessed on 20.09.2023.

Table 1 Raw material specification of the CuBe spring material as provided by the material supplier

Properties	Value	Unit
Young's modulus	120 – 160	GPa
Tensile strength	500 – 1300	GPa
Density	8250	kg/m^3
Coefficient of thermal expansion (CTE)	17*	$\times 10^{-6}/K$
Melting point	860 – 1,000	°C

*At 25 - 300°C. The expansion remains near-linear at colder temperatures until about −100°C (i.e. inside the application range) according to https://www.copper.org/publications/pub_list/pdf/104-5-low-temperatuare.pdf, accessed on 20.09.2023.

Fig. 4 Laser-cut springs. The (later removed) marker on the fourth spring from the right indicates the direction of rolling, which was aligned with the long axis of all cut springs

3.2 Laser cutting

This raw material was then sent to laser cutting. This method was selected to minimise any stress induction to the material. Alternatively, spark erosion cutting was considered; however, to obtain a larger quantity of springs allowing a selection, laser cutting was the faster and more cost-efficient solution. The long axis of the spring was aligned with the indicated rolling direction of the raw material. Like this, the spring bending aligns with the grain direction, providing better spring properties and lower risk of (micro-) cracking.

One additional aspect was altering the material properties due to the heating of the laser. However, the service provider explained that only the edge will be heated with a maximum extent of two times the material thickness, thus here up to 100 microns, and that this might cause a local change in material colour but not its properties. For some samples, small bursts at the spring edges were identified under the microscope after the laser cutting process. Those were removed carefully by hand. Overall, the result was of very good quality, meeting all specified dimensions and tolerances. The cut springs are shown in Fig. 4.

3.3 Heat treatment

After the laser cutting, the raw springs are age hardened by heat treatment at 315°C, not only to increase the yield strength but also to maximise the flatness of the probes. In preparation of the heat treatment, a single blade is placed between two stripes of stainless steel to avoid corrosion. These stripes have thin cuts at the locations where the blade has holes to allow air to escape during the heating process. This stack of stainless steel stripes and blade is then clamped in dedicated flat steel blocks (Fig. 5). Good

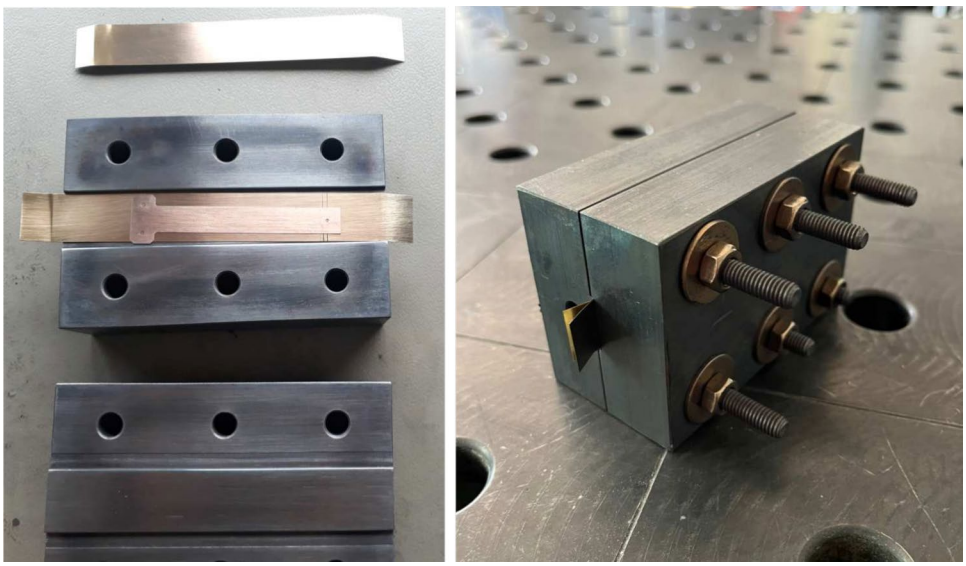

Fig. 5 Left: steel blocks with stainless steel stripes and blade, disassembled. Right: assembled heat-treatment block during cooling on steel table

Fig. 6 Blade on clamping steel block before (top) and after (bottom) heat treatment. The improved straightness (flatness) of the spring is clearly visible

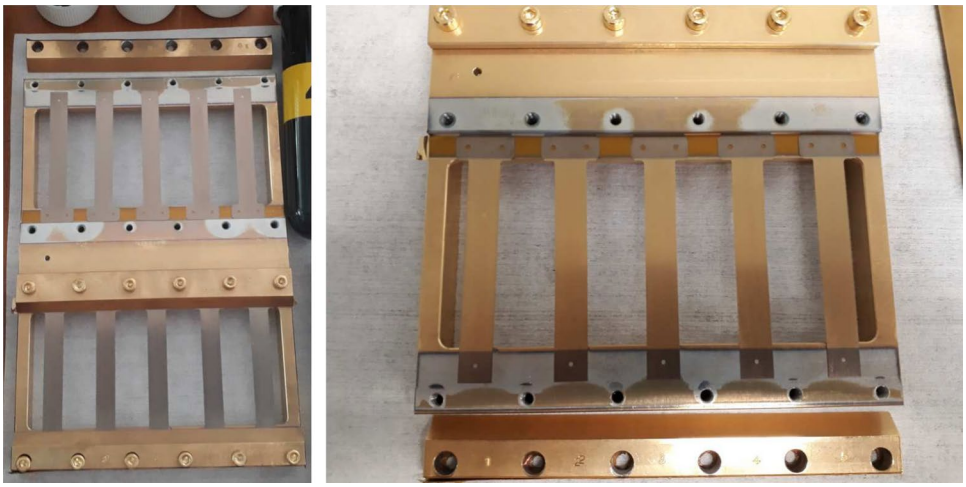

Fig. 7 Blades mounted in a dedicated frame for gold sputtering. Left: Before treatment, the five blades seen on the top are not yet clamped. Right: After treatment, the clamps of the shown blades are already removed to illustrate the difference of the blade surfaces; no gold was deposited on the two ends of each blade

parallel clamping is ensured by applying the same torque on all clamping screws and by verifying the thickness at all four corners of the steel-block assembly which must be the same within a few micrometres. Moreover, the contact surfaces of the two blocks have been grinded. It should be noted that the stainless steel stripes and the steel blocks are thoroughly cleaned [brushing and isopropyl alcohol (IPA) wiping] between each treated blade to remove any dirt and corrosion.

According to the raw material supplier, the precipitation hardening should be done at a temperature of 315°C±15°C. This is indicated for a duration of 2 h by the supplier, but slight improvements can be expected for a duration of 3 h,[2] which was in fact applied. The temperature during the heating is controlled at the location of the blade by inserting a thermal sensor into a dedicated hole in the steel block. Following the heat treatment, the steel-block assembly is air-cooled before taking out the flat blade. A comparison of the spring before and after HT is shown in Fig. 6. The improvement of the straightness of the sensing device is clearly visible. The blades are stored individually in small plastic containers without any additional cleaning until the gold sputtering takes place as presented in the following subsection.

[2] https://www.matthey.ch/fileadmin/user_upload/downloads/Fichiers_PDF/GuideToCopperBeryllium_EN.pdf, accessed on 20.09.2023.

3.4 Gold sputtering

To protect the blade from ageing, e.g., due to oxidation, the blades are protected with a thin layer of gold. In preparation of the gold deposition, ten blades are carefully clamped into a dedicated frame, fixed on both ends (Fig. 7). These two ends correspond to the clamping area of the Macor clamp and the tip masses, respectively. While these regions will not be coated, this is less critical than for the free blade part, i.e., the deforming part of the spring. The layer of gold is applied in vacuum by physical vapour deposition (PVD) with plasma etching prior to starting the process. The plasma etching removes any corrosion on the surface and ensures good adhesion of the gold atoms. The layer deposition thickness is 30–40 nm (50 nm is equal to one thousandth of 50 micron), therefore not influencing the spring behaviour. After this process, the blades are again individually stored in small plastic containers. Storage in nitrogen or vacuum is not required, but is applied whenever possible.

4 Spring assembly integration

With the spring in place, the spring assembly, i.e., with its clamp and tip mass, can be integrated. This section details this process step-by-step and in chronological order. More details on the parts additional to the spring will be provided accordingly.

In the previous section, the formulated straightness requirement of $\pm 5\ \mu m$ was formulated. Not only the spring itself contributes to this requirement, but likewise the integration of the spring inside the cradle as mounting part. In fact, the spring clamp was itself clamped inside the cradle by means of a metal clamp and set screws. Thus, the contact area of the clamp to the cradle was machined with a geometric tolerance of 5 micron parallelism with respect to the contact areas of the electrodes surrounding the spring. A surface finish by grinding with the Macor clamp (Sect. 4.2) pre-integrated with the screws likewise ensured the parallelism of the clamp contact surface to the spring. Adaptations to the centring of the entire spring assembly inside the cradle were realised by shims of thicknesses down to 5 micron.

4.1 Electrical connection

As introduced above, the deflection of the gravimeter spring due to an acceleration (e.g., gravity) is recorded by a capacitive transducer. This requires the blade to be electrically connected to the gravimeter electronics. This is realised by a double twisted wire with PTFE insulation that is soldered directly onto the blade (Fig. 8). A hole of 1 mm diameter has been added to the spring design indicating the electrical connection centre (Fig. 1). For soldering, the blade is placed on a Teflon block and the area to be soldered on is carefully mechanically cleaned from corrosion (recall that this part of the blade is not gold sputtered as described in Sect. 3.4). Soldering is done at 350°C and it is being kept as short as possible to not alter the spring properties. Clearly, the entire electrical connection needs to be maintained inside the 4 mm cutout in the clamping Macor piece, ideally within a circle of max. 3.5 mm to avoid contact in vibration. Structural glue is applied later for protecting the solder joint (Sect. 4.4).

4.2 Macor clamp

After the soldering of the electrical connection, the spring is clamped in the electrically insulating clamping pieces made of Macor. Macor® is a glass-ceramic material with no porosity, it is non-wetting, and it does not deform plastically [13]. Table 2 lists the properties of the material. Therefore, care has to be taken when handling the brittle Macor material,

Table 2 Material properties of Macor®. From https://www.goodfellow.com/de/p/ma80-br-000110/macor-ceramic-bar, accessed on 30.10.2023

Property	Value	Unit
Tensile modulus	67	GPa
Vickers hardness	400	kgf mm^{-2}
Obvious porosity	0.00	%
Density	2.520	g cm^{-3}
Compressive strength	345	MPa
Coefficient of thermal expansion (CTE)	13	$\times 10^{-6} K^{-1}$

Fig. 8 Wired gravimeter spring with soldered connection on the right side

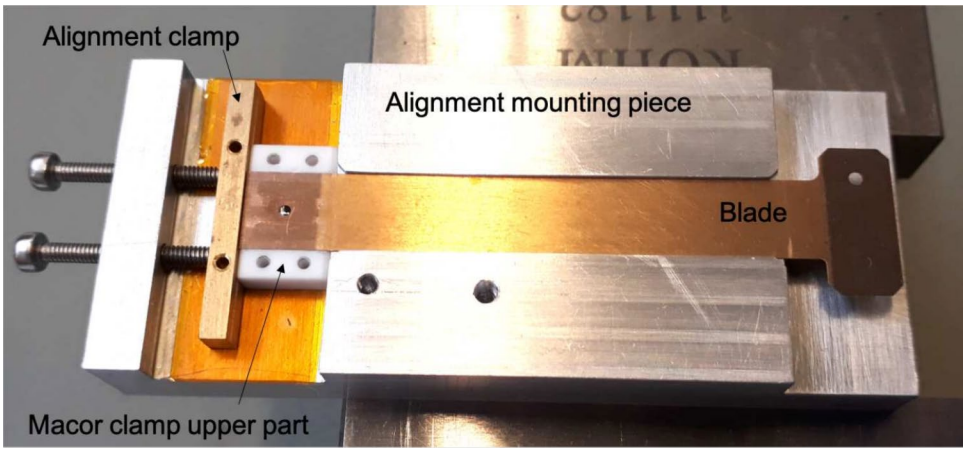

Fig. 9 For the GRASS gravimeter development, a dedicated alignment technique and tool has been developed. The top part of the Macor clamp featuring the hole for the electrical connection is placed on the mounting tool and the blade is placed atop the Macor part and into the alignment mounting piece. Then, by fixing the alignment clamp with the two screws, the macor part and blade are aligned. The alignment clamp has a cutout for the blade, so that the blade will stick out by 100 μm on the left side. Next, the bottom part of the Macor part is placed and the fixation of the Macor clamp is realised with four countersunk M1.2 screws. While the top Macor part provides the hole for access of the electrical connection (Sect. 4.1), the bottom part has two gluing pockets. Using the dedicated alignment mounting piece for the gravimeter blade in combination with the alignment clamp for the Macor, best alignment is ensured

as it can break easily when too much (clamping) force is applied. Next to its insulating properties, it has been selected for the absence of outgassing (after applied bake out), and the very tight achievable machining tolerances [13]. The thermal expansion is relatively low. According to [13], the machining tolerances can be up to 12 micron; the surface finish can be better than 0.5 micron,[3] and the surface can be polished to a smoothness of 0.013 micron. From our experience, working with very experienced machining service providers, machining tolerances better than 5 microns were achieved to support the tight requirements on the straightness of the spring.

The blade has to be placed precisely into the clamping piece, to ensure excellent alignment of the spring inside the clamp, and, therefore, the gravimeter. This is done using a dedicated alignment tool consisting of the alignment mounting piece and an alignment clamp (Fig. 9). Figure 10 shows the Macor pieces, each top and bottom part from both sides. The structural glue (2216) will only be applied after the full assembly of the blade, including tip masses (Sect. 4.4). The alignment of the blade within the Macro clamp is verified with an optical microscope.

4.3 Tip mass

As last part of the assembly, the gravimeter spring tip mass is added to the free-hanging end of the cantilever setup. The tip mass itself consists of two half-masses, two slotted spring pins (DIN 7343 – AiSi302, 1 mm × 12 mm) and eight vespel dampers. The tip mass halves made of tungsten were selected for the high density (Sect. 2); platinum with an ever higher density had to be discarded for budgetary reasons. To maximise the density, near-pure tungsten with a purity of 99.95 % rather than a tungsten alloy had been selected, with a nominal density of $19,300\,\mathrm{kg/m^3}$. Considering the above-mentioned measured mass of one tip mass half of 4.178 g and the (theoretical) CAD volume of the part of $219.7567\,\mathrm{mm^3}$, the actual density of the

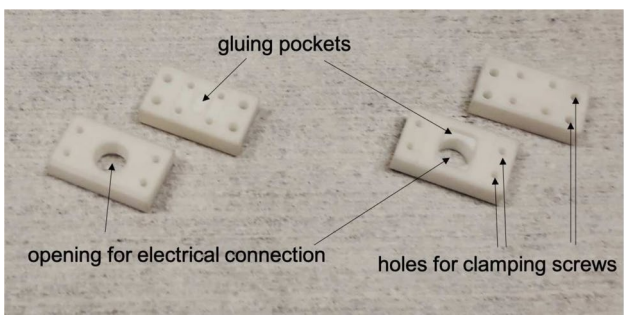

Fig. 10 Top side of Macor clamping piece with circular opening for electrical connection (top and upside down, left), and bottom side of Macor clamping piece (top and upside down, right). On the bottom view of each part, the pockets for glue are visible

[3] The surface finish in [13] is stated "$20\mu m(0.5\mu m)$". Following the pattern of the other provided numbers, first in inch, then in the metric system, the $20\mu m$ must be considered a typo. First, 20 micron is all but a smooth surface quality, and second, 0.5 micron corresponds to (about) 20 micro-inch.

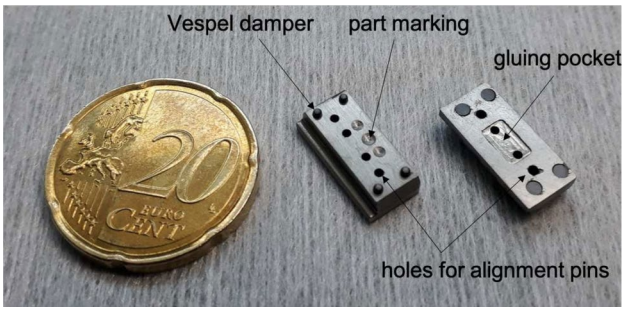

Fig. 11 Both tip mass halves, sandwiching the CuBe spring for fixation. Four dampers are pressed inside each half-tip mass as indicated on the right half. The right piece also shows the glue pocket with two holes for filling. 20 euro cent coin for size reference

material was found to be $19,009\,\mathrm{kg/m^3}$. The machining of the pure tungsten metal, especially the drilling of holes with small diameter (e.g., 1 mm holes for the mentioned spring pins) was a very demanding task for the manufacturer. Unlike Macor, the machinability of tungsten is not very good. Figure 11 shows two tip mass halves. From a batch of manufactured tip masses, for a given spring assembly, two tip masses with the same mass within a few milligrams are paired up. They are inspected together and, if necessary, a tiny amount of material is grinded off, if they do not fit exactly together when preliminary mounted together with the alignment pins. Once a pair is matched, the two halves are marked (increasing number of dots on each half) and the tip masses are weighted again for the record with a calibrated scale.

Next, the vespel dampers are added to each half. Each tip mass half features four holes to insert vespel dampers. A counterbore-design ensures that the dampers cannot move out of the tungsten parts. With the Vespel dampers added to the tip mass, the spring–mass system is damped, avoiding direct metal–metal contact between the tip mass and the spring-mounting piece, surrounding the gravimeter spring. This protects the spring assembly from damage during (launch) vibration and (separation and landing) shock loads. Preventing this metal–metal contact aids further to avoid cold welding in the space environment. For this, first, the dampers are pressed in the two tip mass halves as indicated in Fig. 11. Initially, the pieces stick out too much off the tip mass surfaces. After precise measurement of the cradle, the desired final length of the dampers is calculated so that the gravimeter spring can fully deflect for the anticipated gravity environment with sufficient margin, while any contact of the spring with its surrounding is hindered (Fig. 15). The length of the dampers is adapted by milling them down to the required excess length (Fig. 12).

To integrate the tip mass halves onto the blade, one half is clamped into a precise and flat clamping device (Fig. 13). The achieved precision of the alignment in verified with an optical microscope (Fig. 14). Figure 16 shows the final assembled blade before gluing.

4.4 Gluing

After the blade assembly is completed, its flatness and alignment is again confirmed visually by a microscope. Only then, all parts are fixated using the space-qualified structural Epoxy Adhesive 2216, a product resistive to shock and vibration, and ideal for affixing different materials with each other. To protect the electrical connection, the circular hole in the Macor clamping part harbouring the soldered wire is filled with the epoxy. Furthermore, both the Macor parts and the tip mass halves feature dedicated glue pockets pairs. Filling the glue in one hole, the air can escape via the other hole until the second hole is filled with the injected glue. The glue is inserted with a medical syringe. First, one side

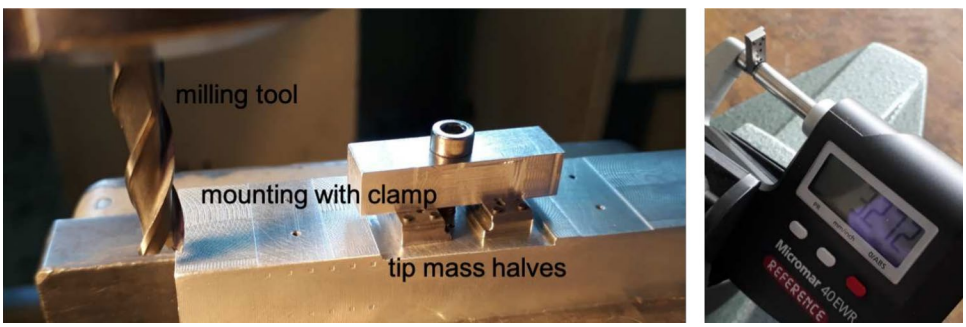

Fig. 12 Left: two tip mass halves clamped on an aluminium mounting piece for accurate shortening by milling of vespel dampers. Before placing the tip mass halves, the contact area of this mounting piece with the tip masses is milled down by a few micrometres prior to mounting the parts, ensuring complete flatness and parallelism of the setup. This step has to be repeated in case the mounting piece is removed from the milling machine. Subsequently, the tip mass halves are clamped on the mounting pieces and the Vespel dampers are milled down to the desired (excess) length. The precision achieved is better than 5 μm. Right: measurement of final length with calibrated micrometre following the shortening procedure

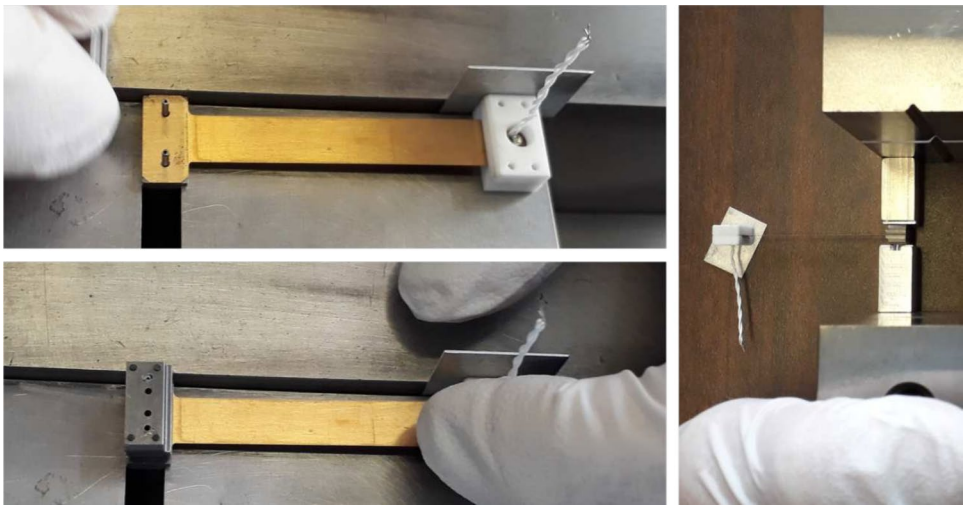

Fig. 13 Tip mass integration onto the blade. Upper-left: two DIN 7343-AISI302 1 mm × 12 mm slotted spring pins are then pressed into the foreseen holes. The blade is carefully placed onto the clamping device while inserting the pins of the tip mass into the holes of the blade. Bottom-left: to account for the difference in width of Macor clamp and tip mass, a shim with the difference in width (0.5 mm, see Fig. 1) is placed to align the blade strictly perpendicular on the device. Subsequently, the second half of the tip mass is added and pressed onto the pins by hand. Right: To insert the pins completely into the tip masses, the tip mass end of the assembled blade is clamped into a special tool that avoids touching the vespel dampers while pressing the pins into the tip mass

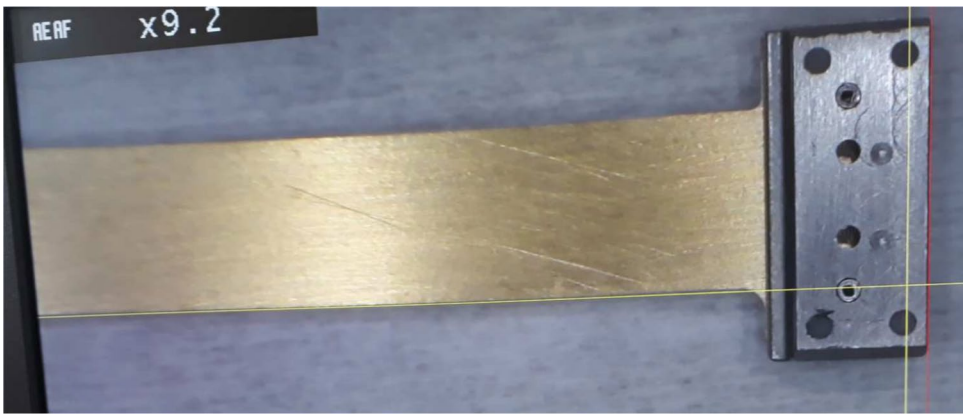

Fig. 14 Alignment control of tip mass on blade seen with optical microscope

of the blade assembly is glued (Fig. 17). After a curing time of about 48 h at room temperature, the assembly is turned, and finally, the other side is glued (Fig. 18). With this, the spring assembly is completed and ready to be integrated into the cradle and then into the GRASS gravimeter instrument.

5 Future work

The here-presented gravimeter spring design is specifically designed for the GRASS gravimeter on-board the Juventas deep space CubeSat, forming part in the ESA Hera mission that was launched on 7 October 2024. The dimensions as laid out here were primarily derived from limitations of the overall allocated instrument volume. Regarding future missions, and depending on the gravity environment, it will be possible to either maintain the here-presented spring design or to perform adaptations. For example, if the volume constraints allow it, the overall spring length or tip mass volume (and therefore mass) could be increased, e.g., to increase further the instrument sensitivity. One potential option to use the here-presented spring design would be a surface measurement on (99942) Apophis, a near-Earth object (NEO) that will pass Earth safely but very closely on 13 April 2029.

To reduce the deflection, e.g., for missions to the Moon or Mars, it will be possible to increase the spring thickness, to adapt to the increased surface gravity accordingly. Using the gravimeter on the Moon with a specific focus on intact lava tubes, differentially measuring from above and inside the lava tube was first proposed by [14]. Similarly, a rover-based survey to detect intact lava tubes was presented by [15]. More recently, this option is being studied as part of the

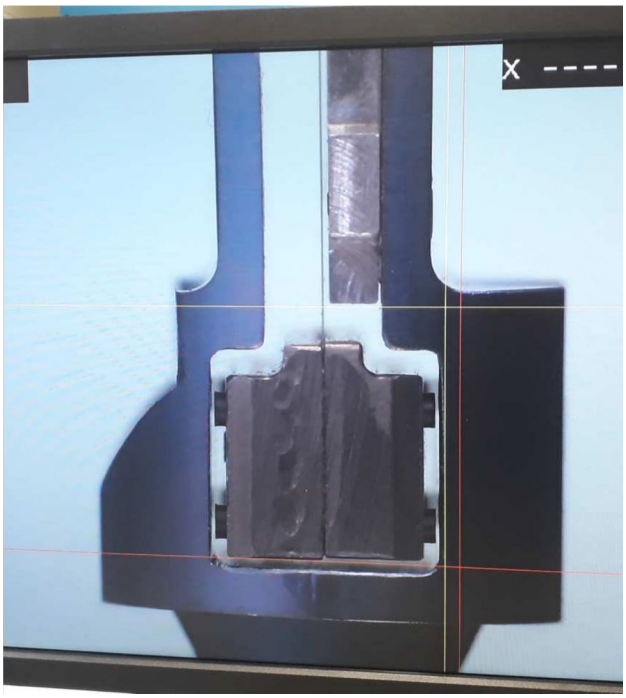

Fig. 15 Spring assembly with tip mass and inserted dampers inside the cradle (blue) as spring-mounting piece. In the pictured vertical setup, clear gaps on both sides of the dampers towards the cradle are visible; they measure around 70 μm. The gap on the right side of the blade to the inserted aluminium piece amount to around 150 μm. Picture taken with optical microscope

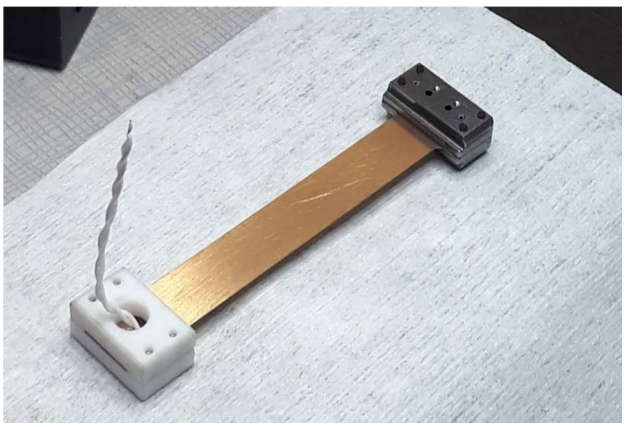

Fig. 16 Integrated blade assembly before gluing

LunarLeaper proposal [16], an ESA small mission candidate to explore lunar caves.

Without question, further applications of the GRASS spring can be considered, e.g., for seismic or acceleration measurements.

Rovers or landers with more available volume could thus accommodate a larger version of the instrument, with a larger spring, while maintaining the rectangular bending spring concept. Such larger gravimeter with similar, yet larger spring had been studied [10] for the DLR/CNES Phobos rover to be deployed by the JAXA Martian Moon eXplorer (MMX) mission [17].

Adaptations to gravity environments even smaller than Dimorphos will be, however, challenging. The machining tolerances set a natural boundary in the achievable spring alignment and electrode separation. Because of this, it would for example not be possible to constantly increase the spring length to further increase the spring deflection, as the required alignment cannot be ensured at a arbitrarily long overall length.

6 Conclusion

This work has presented the GRASS gravimeter spring design and design constraints for the Juventas CubeSat to land on Dimorphos as part of the ESA Hera mission, launched on 7 October 2024. In the absence of a controlled landing attitude and gravity vector orientation knowledge, a cantilever-like bending spring has been developed, providing largest sensitivity in one direction while remaining insensitive in the two other dimensions. For this novel spring design, the step-by-step manufacturing has been presented. Copper Beryllium (CuBe) was selected for the spring manufacturing, providing excellent spring properties. Cutting the raw material by laser cutting provided excellent results without altering the material properties while providing very good geometric tolerances. Moreover, the heat treatment and gold sputtering processes have been introduced and explained, complementing the final gravimeter spring production. A step-by-step description of the gravimeter spring assembly shows how best alignment and fixation of the device is ensured, using an alignment tool and glue, respectively. Future work will allow to adapt the here-presented gravimeter spring design accordingly, accounting for different gravities, allowing to perform gravity surveys throughout our Solar System.

Fig. 17 Left: blade with tip mass and glue-filled syringe before application of epoxy. Middle: tip mass after gluing. Right: Macor clamp after gluing

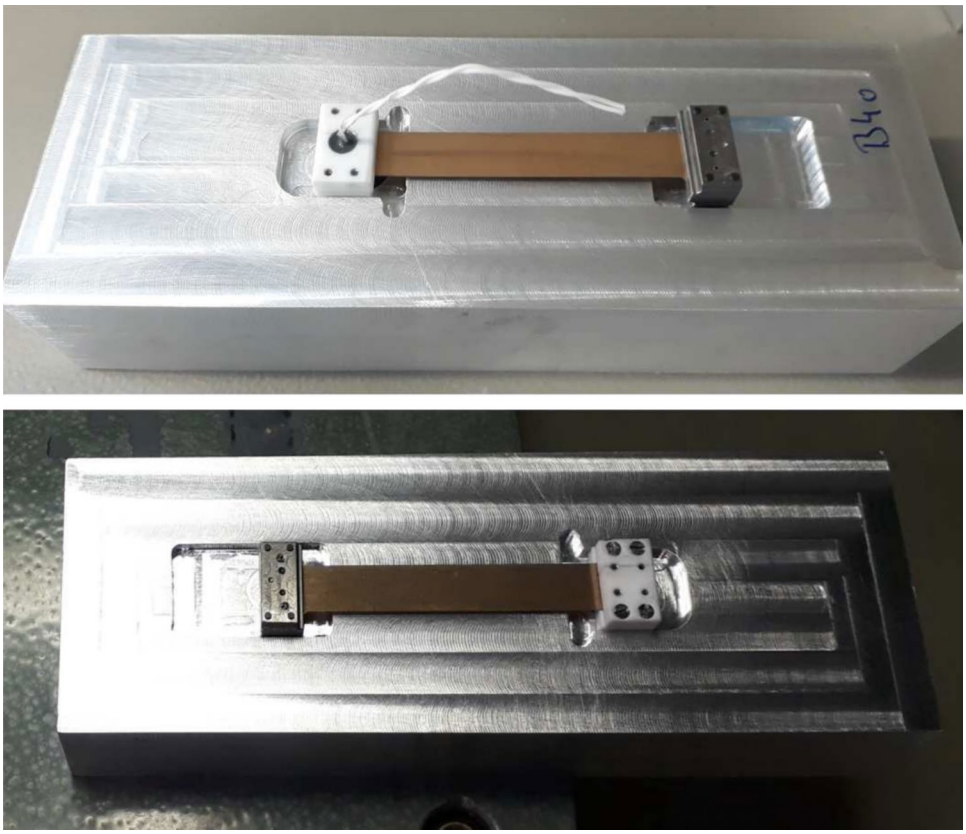

Fig. 18 Fully assembled and glued blade, top and bottom view

Acknowledgements This work received funding by the BELgian federal Science Policy Office (BELSPO) via the PROgramme for the Development of scientific EXperiments (PRODEX) by the European Space Agency (ESA) under Contract No. 4000138600. MN acknowledges funding from the Foundation of German Business (sdw) and the Royal Observatory of Belgium (ROB) PhD grants. The authors specially thank the technical and engineering team of the Belgian Royal Institute of Space Aeronomy (BIRA-IASB) for the extensive support and the possibility to use their facilities and equipment.

Author Contributions MN and EVR worked on the spring design and discussed the implications of critical design parameters on the science case of the instrument with BR and ÖK. For the spring manufacturing, the raw material acquisition, laser cutting, and gold sputtering were managed by MN, while the heat treatment was performed in-house by

BR and EVR. The spring assembly integration was performed by EVR and BR. MN and BR wrote the main manuscript text, and EVR and ÖK critically reviewed the manuscript. Figures 1, 2, and 4 were prepared by MN; Fig. 3 by EVR; and Figs. 5 through 18 by BR. ÖK was responsible for the overall planning and supervision of the work. All authors agree to be accountable for the content of the work.

Data availability Not applicable.

Declarations

Conflict of interest The authors declare that they have no conflict of interest.

References

1. Giganti, J.J., Larson, J., Richard, J., Weber, J.: 12. Lunar Surface Gravimeter Experiment. Apollo 17: Preliminary Science Report **330** (1973)
2. Talwani, M., Thompson, B.D., Dent, B., Kahle, H.-G., Buck, S.: 13. Traverse Gravimeter Experiment. Apollo 17: Preliminary Science Report **330** (1973)
3. Lewis, K.W., Peters, S., Gonter, K., Morrison, S., Schmerr, N., Vasavada, A.R., Gabriel, T.: A surface gravity traverse on Mars indicates low bedrock density at Gale crater. Science **363**(6426), 535–537 (2019)
4. Goldberg, H.R., Karatekin, Ö., Ritter, B., Herique, A., Tortora, P., Prioroc, C., Gutierrez, B.G., Martino, P., Carnelli, I.: The Juventas cubesat in support of ESA's hera mission to the asteroid Didymos (2019)
5. Michel, P., Küppers, M., Bagatin, A.C., Carry, B., Charnoz, S., De Leon, J., Fitzsimmons, A., Gordo, P., Green, S.F., Hérique, A.: The ESA Hera mission: detailed characterization of the DART impact outcome and of the binary asteroid (65803) Didymos. Planetary Sci. J. **3**(7), 160 (2022)
6. Karatekin, O., Moreno Villa, V.M., Goldberg, H., : Preliminary investigation of the Juventas CubeSat landing on asteroid Dimorphos. In: European Planetary Science Congress, pp. 2020–683 (2020)
7. Biele, J., Ulamec, S., Maibaum, M., Roll, R., Witte, L., Jurado, E., Muñoz, P., Arnold, W., Auster, H.-U., Casas, C.: The landing (s) of Philae and inferences about comet surface mechanical properties. Science **349**(6247), 9816 (2015)
8. Noeker, M., Van Ransbeeck, E., Ritter, B., Karatekin, Ö.: The GRASS Gravimeter Rotation Mechanism for ESA Hera Mission On-Board Juventas Deep Space CubeSat. In: Proceedings of the 46th Aerospace Mechanisms Symposium, Virtual, pp. 159–172 (2022)
9. Noeker, M.: Surface gravity modelling and space gravimeter development in the context of solar system small bodies. PhD thesis, UCL-Université Catholique de Louvain (2023)
10. Noeker, M., Van Ransbeeck, E., Karatekin, O., Ritter, B.: Development of a compact payload mechanism enabling continuous motorized sensor head rotation and signal transfer. ESMATS 2021 **19**(18) (2021)
11. Hamacher, H., Richter, H.-E., Drees, S.: A system to measure absolute low frequency acceleration on the International Space Station. In: IMTC/99. Proceedings of the 16th IEEE Instrumentation and Measurement Technology Conference (Cat. No. 99CH36309), vol. 1, pp. 249–253 (1999). IEEE
12. Young, W.C., Budynas, R.G., Sadegh, A.M.: Roark's Formulas for Stress and Strain. McGraw-Hill Education, New York City (2012)
13. Dabnun, M.A., Hashmi, M., El-Baradie, M.: Surface roughness prediction model by design of experiments for turning machinable glass-ceramic (Macor). J. Mater. Process. Technol. **164**, 1289–1293 (2005)
14. Noeker, M., Karatekin, Ö., Ritter, B.: Accessing the Lunar Underground: The LAva-TUbe iNvestigAtion (LA-TUNA) Mission Concept. In: 52nd Lunar and Planetary Science Conference, p. 1574 (2021)
15. de Veld, F., Saadia, B., Birkett, S., Braun, A.: Grasimu: A software toolbox for gravity modelling and survey design in lunar exploration. In: 52nd Lunar and Planetary Science Conference, p. 1814 (2021)
16. Ritter, B., Karatekin, Ö., Mittelholz, A., Stähler, S.C.: Exploring subsurface extent and physical properties of lunar lava tubes using surface microgravity survey. Technical report, Copernicus Meetings (2024)
17. Ulamec, S., Michel, P., Grott, M., Böttger, U., Hübers, H.-W., Murdoch, N., Vernazza, P., Özgür, K., Knollenberg, J., Willner, K., : A rover for the JAXA MMX Mission to Phobos. In: 70th International Astronautical Congress, IAC 2019, p. 19 (2019). International Astronautical Federation